

# Cross sections for low-energy $\pi^- \gamma$ reactions

N. Kaiser and J.M. Friedrich

Physik-Department, Technische Universität München, D-85747 Garching, Germany

## Abstract

We review the cross sections for low-energy  $\pi^- \gamma$  reactions in the framework of chiral perturbation theory. Charged pion Compton scattering,  $\pi^- \gamma \rightarrow \pi^- \gamma$ , is considered up to one-loop order where the pion's internal structure enters through the difference of the electric and magnetic pion polarizability,  $\alpha_\pi - \beta_\pi$ . The ongoing COMPASS experiment aims at measuring this important structure constant with high statistics using the Primakoff effect. In the same way, the reaction  $\pi^- \gamma \rightarrow \pi^- \pi^0$  serves as a test of the QCD chiral anomaly (via the  $\gamma 3\pi$ -coupling constant  $F_{\gamma 3\pi}$ ). Furthermore, we calculate the total cross sections for neutral and charged pion-pair production,  $\pi^- \gamma \rightarrow \pi^- \pi^0 \pi^0$  and  $\pi^- \gamma \rightarrow \pi^- \pi^+ \pi^-$ , which are governed by the chiral  $\pi\pi$ -interaction. Finally, we investigate the radiative (correction) process  $\pi^- \gamma \rightarrow \pi^- \gamma \gamma$  and calculate the corresponding two-photon mass spectrum. This information will be useful for analyzing the  $\pi^-$  Primakoff scattering events with photons in the final state.

PACS: 12.20.Ds, 12.39.Fe, 13.60.Fz, 13.75.Lb

## 1 Introduction and summary

The pions ( $\pi^+$ ,  $\pi^0$ ,  $\pi^-$ ) are the Goldstone bosons of spontaneous chiral symmetry breaking in QCD:  $SU(2)_L \times SU(2)_R \rightarrow SU(2)_V$ . Their low-energy dynamics can therefore be calculated systematically (and accurately) with chiral perturbation theory in form of a loop-expansion based on an effective chiral Lagrangian. The very accurate two-loop prediction [1] for the isospin-zero S-wave  $\pi\pi$ -scattering length  $a_0^0 = (0.220 \pm 0.005)m_\pi^{-1}$  has recently been confirmed in the E865 experiment [2] at BNL by analyzing the  $\pi^+\pi^-$  invariant mass distribution of the rare kaon decay mode  $K^+ \rightarrow \pi^+\pi^-e^+\nu_e$ . One particular implication of that good agreement between theory and experiment is that the quark condensate  $\langle 0|\bar{q}q|0\rangle$  constitutes the leading order parameter [3] of spontaneous chiral symmetry breaking (considering the two-flavor sector of QCD). As a consequence, one can assert that more than 94% of the pion mass,  $m_\pi = 139.57$  MeV, must stem from the quark condensate [3]. Furthermore, the DIRAC experiment [4] at CERN has been proposed to determine the difference of the isospin-zero and isospin-two S-wave  $\pi\pi$ -scattering lengths  $a_0^0 - a_0^2$  by measuring the life time ( $\tau \simeq 3$  fs) of pionium (i.e.  $\pi^+\pi^-$  bound electromagnetically and decaying into  $\pi^0\pi^0$ ). In the meantime the NA48/2 collaboration [5] at CERN has accumulated very high statistics for the charged kaon decay modes  $K^\pm \rightarrow \pi^\pm\pi^0\pi^0$ , which allowed them to extract the value  $a_0^0 - a_0^2 = (0.268 \pm 0.010)m_\pi^{-1}$  for the  $\pi\pi$ -scattering length difference from the cusp effect in the  $\pi^0\pi^0$  mass spectrum at the  $\pi^+\pi^-$  threshold. This experimental result is again in very good agreement with the two-loop prediction  $a_0^0 - a_0^2 = (0.265 \pm 0.004)m_\pi^{-1}$  of chiral perturbation theory [1]. For a discussion of isospin breaking corrections which have to be included in a meaningful comparison between theory and experiment, see also ref.[6]. Clearly, these remarkable confirmations give confidence that chiral perturbation theory is the correct framework to calculate reliably and accurately the strong interaction dynamics of the pions at low energies.

Electromagnetic processes offer further possibilities to probe the internal structure of the pion. Whereas the charge (or vector) form factor of the pion,  $F_\pi(t)$ , is largely dominated by the low-lying  $\rho(770)$ -resonance, pion Compton scattering  $\pi^- \gamma \rightarrow \pi^- \gamma$  allows one to extract the electric and magnetic polarizabilities of the (charged) pion. In a classical picture these polarizabilities characterize the deformation response (i.e. induced dipole moments) of a composite system in external electric and magnetic fields. In the proper quantum field theoretical formulation the electric and magnetic polarizabilities,  $\alpha_\pi$  and  $\beta_\pi$ , are defined as expansion coefficients of the Compton scattering amplitudes at threshold. Since pion targets are not directly available, real pion Compton scattering has been approached using different artifices, such as high-energy pion-nucleus bremsstrahlung  $\pi^- Z \rightarrow \pi^- Z \gamma$  [7], radiative pion production off the proton  $\gamma p \rightarrow \gamma \pi^+ n$  [8], and the crossed channel two-photon reaction  $\gamma \gamma \rightarrow \pi^+ \pi^-$  as embedded in the  $e^+ e^- \rightarrow e^+ e^- \pi^+ \pi^-$  process [9]. The corresponding results for the electric and magnetic pion polarizabilities scatter substantially and they have also large uncertainties. On the other hand, chiral perturbation theory at two-loop order gives the firm prediction  $\alpha_\pi - \beta_\pi = (5.7 \pm 1.0) \cdot 10^{-4} \text{ fm}^3$  [10] for the polarizability difference. It is however in conflict with the existing experimental results from Serpukhov  $\alpha_\pi - \beta_\pi = (13.6 \pm 3.7) \cdot 10^{-4} \text{ fm}^3$  [7] and MAMI  $\alpha_\pi - \beta_\pi = (11.6 \pm 3.4) \cdot 10^{-4} \text{ fm}^3$  [8] which amount to values more than twice as large. The result  $\alpha_\pi - \beta_\pi = (4.8 \pm 1.0) \cdot 10^{-4} \text{ fm}^3$  [9] from the MARK II experiment is consistent with the chiral prediction, but the corresponding low-energy cross sections for  $\gamma \gamma \rightarrow \pi^+ \pi^-$  are (within their errorbars) rather insensitive to even sizeable changes of the pion polarizabilities [11]. We also note that radiative pion photoproduction  $\gamma p \rightarrow \gamma \pi^+ n$  has recently been analyzed in the framework of heavy baryon chiral perturbation theory [12]. It has been found in ref.[12] that additional contributions from  $\gamma \gamma \pi N N$  vertices in the chiral Lagrangian  $\mathcal{L}_{\pi N}^{(3)}$  can have effects on the cross section which are comparable to those of the pion polarizabilities. A larger coverage of the photon scattering angle and other kinematical variables is therefore required in order to disentangle more cleanly the pion pole term and the residual radiative pion photoproduction amplitude.

In that situation, it is very promising that the ongoing COMPASS experiment [13] at CERN aims at measuring the pion polarizabilities,  $\alpha_\pi$  and  $\beta_\pi$ , with high statistics using the Primakoff effect. The scattering of high-energy negative pions in the Coulomb field of a heavy nucleus (of charge  $Z$ ) gives access to cross sections for  $\pi^- \gamma$  reactions through the equivalent photon method:

$$\frac{d\sigma}{ds dt dQ^2} = \frac{Z^2 \alpha}{\pi (s - m_\pi^2)} \frac{Q^2 - Q_{min}^2}{Q^4} \frac{d\sigma_{\pi^- \gamma}}{dt}, \quad Q_{min} = \frac{s - m_\pi^2}{2E_{\text{beam}}}. \quad (1)$$

Here,  $\sqrt{s} > m_\pi$  is the  $\pi^- \gamma$  center-of-mass energy and  $t < 0$  the squared invariant momentum transfer between the initial and final state pion.  $Q$  denotes the momentum transferred by the virtual photon to the heavy nucleus and one aims at isolating the Coulomb peak  $Q \rightarrow 0$  from the strong interaction background. Due to the small range of  $Q \approx 0$  the nuclear charge form factor can be approximated by  $F_Z(Q^2) \simeq Z$ . A first pilot run performed at COMPASS has already accumulated statistics for Primakoff events comparable to previous experiments of this type [7, 14]. For a recent discussion of possible problems (nuclear scattering, kinematical limitations etc.) associated with isolating the Coulomb peak, see refs.[15, 16].

The purpose of the present paper is to review the cross sections for various low-energy  $\pi^- \gamma$  reactions in the framework of chiral perturbation theory. We treat pion Compton scattering,  $\pi^- \gamma \rightarrow \pi^- \gamma$ , up to one-loop order, where the pion's internal structure appears for the first time in form of the difference of the electric and magnetic polarizability,  $\alpha_\pi - \beta_\pi$ . In the view the expected accuracy of the COMPASS experiment, and the knowledge that two-loop corrections [10] are relatively small, this approximation should be sufficient. Then, we consider (at one-loop order) the reaction  $\pi^- \gamma \rightarrow \pi^- \pi^0$  which is also under study in the COMPASS experiment. It

serves as a test of the QCD chiral anomaly via measuring the  $\gamma 3\pi$ -coupling constant  $F_{\gamma 3\pi}$ . As the pertinent one-loop amplitudes are available from the literature, we restrict here ourselves to a concise but explicit presentation of the relevant cross section formulas. Actually new is our calculation of total cross sections for neutral and charged pion-pair production,  $\pi^- \gamma \rightarrow \pi^- \pi^0 \pi^0$  and  $\pi^- \gamma \rightarrow \pi^- \pi^+ \pi^-$ , which interestingly are determined by the chiral  $\pi\pi$ -interaction. With the larger data sample planned in future COMPASS runs sufficient statistics will become available for these reactions. Finally, we investigate the radiative correction process  $\pi^- \gamma \rightarrow \pi^- \gamma \gamma$  and calculate the corresponding two-photon mass spectrum. This information will be helpful for analyzing the  $\pi^-$  Primakoff scattering events with photons in the final state.

## 2 Charged pion Compton scattering

We start with the process of Compton scattering off a negatively charged pion:  $\pi^-(p_1) + \gamma(k_1, \epsilon_1) \rightarrow \pi^-(p_2) + \gamma(k_2, \epsilon_2)$ . The corresponding T-matrix in the center-of-mass frame has (in Coulomb gauge  $\epsilon_{1,2}^0 = 0$ ) the form:

$$T_{\pi\gamma} = 8\pi\alpha \left\{ -\vec{\epsilon}_1 \cdot \vec{\epsilon}_2 A(s, t) + \vec{\epsilon}_1 \cdot \vec{k}_2 \vec{\epsilon}_2 \cdot \vec{k}_1 \frac{2}{t} [A(s, t) + B(s, t)] \right\}, \quad (2)$$

with  $\alpha = 1/137.036$  the fine-structure constant and  $s = (p_1 + k_1)^2 > m_\pi^2$  and  $t = (k_1 - k_2)^2 < 0$  the independent Mandelstam variables. Performing the sums over transversal polarizations and applying flux and appropriate phase space factors, the resulting differential cross section reads:

$$\frac{d\sigma}{d\Omega_{\text{cm}}} = \frac{\alpha^2}{2s} \left\{ |A(s, t)|^2 + |A(s, t) + (1+z)B(s, t)|^2 \right\}, \quad (3)$$

with  $t = (s - m_\pi^2)^2(z - 1)/2s$  where  $z = \cos \theta_{\text{cm}} = \hat{k}_1 \cdot \hat{k}_2$  is the cosine of the cms scattering angle. The decomposition in eq.(2) into two invariant amplitudes  $A(s, t)$  and  $B(s, t)$  has been done with hindsight to an expression as simple as possible for the (unpolarized) differential cross.

The amplitudes at tree level coincide with the ones from scalar quantum electrodynamics:

$$A(s, t)^{(\text{tree})} = 1, \quad B(s, t)^{(\text{tree})} = \frac{s - m_\pi^2}{m_\pi^2 - s - t}. \quad (4)$$

Note that the contribution of the  $s$ -channel pole diagram vanishes in Coulomb gauge since the coupling of the initial state photon becomes zero in that gauge,  $\epsilon_1 \cdot (2p_1 + k_1) = 0$ . The one-pion loop diagrams of chiral perturbation theory generate, after renormalization of the pion mass  $m_\pi$ , the following (finite) contribution to the Compton amplitude  $A(s, t)$  [10, 17]:

$$A(s, t)^{(\text{loop})} = -\frac{1}{(4\pi f_\pi)^2} \left\{ \frac{t}{2} + 2m_\pi^2 \ln^2 \frac{\sqrt{4m_\pi^2 - t} + \sqrt{-t}}{2m_\pi} \right\}, \quad (5)$$

with  $f_\pi = 92.4$  MeV the pion decay constant. Heuristically, it can be interpreted as the (leading) correction arising from photon scattering off the "pion cloud around the pion". The internal structure of the pion enters through its electric and magnetic polarizabilities, which obey at the one-loop order the constraint  $\alpha_\pi + \beta_\pi = 0$  [18]. The pertinent  $\gamma\gamma\pi\pi$  contact vertices from the chiral Lagrangian  $\mathcal{L}_{\pi\pi}^{(4)}$  give rise to the contribution [10, 17]:

$$A(s, t)^{(\text{pola})} = -\frac{\beta_\pi m_\pi t}{2\alpha}, \quad \alpha_\pi - \beta_\pi = \frac{\alpha(\bar{l}_6 - \bar{l}_5)}{24\pi^2 f_\pi^2 m_\pi}, \quad (6)$$

to the Compton amplitude  $A(s, t)$ . The relevant combination of low-energy constants  $\bar{l}_6 - \bar{l}_5$  can be extracted from the axialvector-to-vector form factor ratio  $h_A/h_V = 0.443 \pm 0.015 = (\bar{l}_6 - \bar{l}_5)/6 + \mathcal{O}(m_\pi^2)$  measured in the PIBETA experiment [19] at PSI via the radiative pion decay  $\pi^+ \rightarrow e^+ \nu_e \gamma$ . The two-loop analysis of ref.[20] yields the value  $\bar{l}_6 - \bar{l}_5 = 3.0 \pm 0.3$  implying the pion polarizability difference:  $\alpha_\pi - \beta_\pi \simeq 6.0 \cdot 10^{-4} \text{ fm}^3$ . It should be stressed that the current-algebra relation  $\alpha_\pi - \beta_\pi = \alpha h_A / (4\pi^2 h_V f_\pi^2 m_\pi) + \mathcal{O}(m_\pi)$  constitutes a low-energy theorem [18] which must hold (to leading order) in any chiral invariant theory. From this point of view, the parametrization of  $\alpha_\pi - \beta_\pi$  in terms of a phenomenological  $\sigma$ -meson exchange, as chosen in ref.[16], is problematic since it ignores that profound theoretical constraint. Moreover, as stressed in ref.[18] the outcome  $\bar{l}_6 - \bar{l}_5 = -2$  of the chiral invariant linear  $\sigma$ -model is completely ruled out by experiment, because it leads to an axialvector-to-vector form factor ratio  $h_A/h_V$  of the wrong sign. As a matter of fact, the actual physics behind the low-energy constant  $\bar{l}_6 - \bar{l}_5$  is the excitation of vector and axialvector meson resonances [18]. In the same way the existing experimental determinations of  $\alpha_\pi - \beta_\pi \simeq 12 \cdot 10^{-4} \text{ fm}^3$  [7, 8] give reason to doubts since they violate the chiral low-energy theorem notably by a factor 2. In order to clarify the situation on the theoretical side, a complete two-loop calculation of pion polarizabilities has been performed in ref.[10, 17], grinding out the analytical result:

$$\begin{aligned} \alpha_\pi - \beta_\pi = & \frac{\alpha(\bar{l}_6 - \bar{l}_5)}{24\pi^2 f_\pi^2 m_\pi} + \frac{\alpha m_\pi}{(4\pi f_\pi)^4} \left\{ c^r + \frac{8}{3} \left( \bar{l}_2 - \bar{l}_1 + \bar{l}_5 - \bar{l}_6 + \frac{65}{12} \right) \ln \frac{m_\pi}{m_\rho} \right. \\ & \left. + \frac{4}{9} (\bar{l}_1 + \bar{l}_2) - \frac{\bar{l}_3}{3} + \frac{4\bar{l}_4}{3} (\bar{l}_6 - \bar{l}_5) - \frac{187}{81} + \left( \frac{53\pi^2}{48} - \frac{41}{324} \right) \right\}, \end{aligned} \quad (7)$$

expressed in terms of the chiral low-energy constants  $\bar{l}_1 = -0.4 \pm 0.6$ ,  $\bar{l}_2 = 4.3 \pm 0.1$ ,  $\bar{l}_3 = 2.9 \pm 2.4$ ,  $\bar{l}_4 = 4.4 \pm 0.2$ . The last term proportional to  $53\pi^2/48 - 41/324$  stems from the nonfactorizable acnode diagrams. The additional counterterm  $c^r$  has been estimated via resonance saturation as  $c^r \simeq 0$  [10] and we have set the scale in the chiral logarithm  $\ln(m_\pi/m_\rho)$  equal to the  $\rho$ -meson mass  $m_\rho = 770 \text{ MeV}$ . Taking into account various theoretical uncertainties the two-loop prediction amounts to:  $\alpha_\pi - \beta_\pi = (5.7 \pm 1.0) \cdot 10^{-4} \text{ fm}^3$  [10]. As this value is fully compatible with the current-algebra result, it is now assured that there are no significant corrections to the chiral low-energy theorem for the pion polarizability difference  $\alpha_\pi - \beta_\pi$ . For a more detailed discussion of these issues, see ref.[10]. The non-vanishing two-loop prediction for the pion polarizability sum,  $\alpha_\pi + \beta_\pi = 0.16 \cdot 10^{-4} \text{ fm}^3$  [10], is in fact consistent with results from dispersion sum rules [11] but presumably much too small to cause an observable effect in pion Compton scattering. Moreover, as indicated e.g. by Fig. 6 in ref.[10] the one-loop approximation should be sufficient for low energies  $\sqrt{s} < 4m_\pi$ .

Fig. 1 shows the calculated total cross section  $\sigma_{\text{tot}}(s)$  for  $\pi^-$  Compton scattering in the low-energy region  $m_\pi < \sqrt{s} < 3.5m_\pi$ . At higher energies the excitation of the broad  $\rho(770)$ -resonance becomes prominent ( $m_\rho \simeq 5.5m_\pi$ ). One observes that the one-loop result is almost indistinguishable from the cross section for a point-like pion:

$$\sigma_{\text{tot}}(s)^{(\text{pt})} = \frac{4\pi\alpha^2(s + m_\pi^2)}{s(s - m_\pi^2)^3} \left[ s^2 - m_\pi^4 - 2sm_\pi^2 \ln \frac{s}{m_\pi^2} \right]. \quad (8)$$

The effects from the pion's low-energy structure (pion-loops and electric minus magnetic polarizability) contribute at the level of only 1%. This finding is of course not entirely new [17].

The angular dependence of the differential cross section  $d\sigma/d\Omega_{\text{cm}}$  is shown in Fig. 2 for three selected center-of-mass energies,  $\sqrt{s} = (2, 3, 4) m_\pi$ . The full curves are calculated with (assumed) pion polarizabilities  $\alpha_\pi = -\beta_\pi = 3.0 \cdot 10^{-4} \text{ fm}^3$  and the dashed lines correspond to

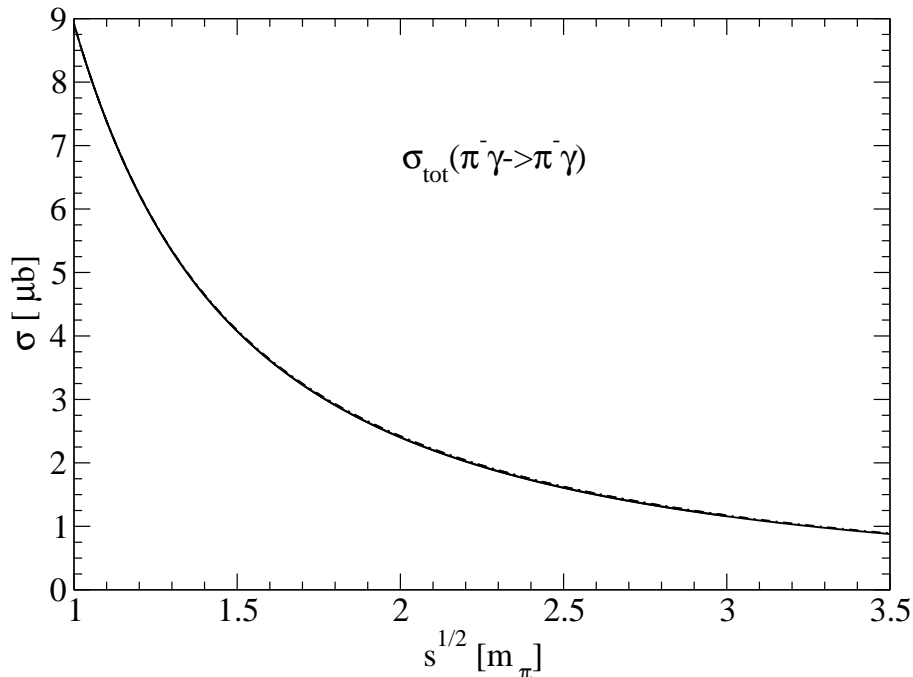


Figure 1: Total elastic cross section for charged pion Compton scattering. Effects from the pion’s low-energy structure (pion-loops and polarizability difference  $\alpha_\pi - \beta_\pi$ ) contribute at the level of 1%.

the case of a structureless pion:

$$\frac{d\sigma^{(\text{pt})}}{d\Omega_{\text{cm}}} = \frac{\alpha^2[s^2(1+z)^2 + m_\pi^4(1-z)^2]}{s[s(1+z) + m_\pi^2(1-z)]^2}, \quad (9)$$

where  $z = \cos \theta_{\text{cm}}$ . One gets instructed that the effects of the pion’s low-energy structure on observables are rather tiny. They amount merely to a few percent reduction of the differential cross section in backward directions,  $z \approx -1$ . This gives some impression of the enormous experimental challenge posed for measuring with good accuracy the pion polarizabilities. First, low-energy  $\pi^- \gamma$  cross sections (e.g.  $\sqrt{s} < 4m_\pi$ ) need to be extracted from the Primakoff events under the Coulomb peak. Secondly, these must come with an accuracy such that the marginal deviations from the point-like cross section become statistically significant. We also note that the (quadratic) pion-loop contribution  $A(s, t)^{(\text{loop})} \sim t^2 + \dots$  in eq.(5) works against the (linear) polarizability term  $A(s, t)^{(\text{pola})} \sim t$ . Therefore, leaving it out in an analysis of pion Compton scattering data would lead to an underestimation of the pion polarizabilities  $\alpha_\pi \simeq -\beta_\pi > 0$ . In the optimal case their fitted value should also be independent of the upper limit put on the center-of-mass energy  $\sqrt{s}$ .

### 3 Chiral anomaly test

Next, we come to the neutral pion production reaction  $\pi^-(p_1) + \gamma(k, \epsilon) \rightarrow \pi^-(p_2) + \pi^0(p_0)$ . The corresponding T-matrix:

$$T_{\gamma 3\pi} = \frac{e}{4\pi^2 f_\pi^3} \epsilon_{\mu\nu\kappa\lambda} \epsilon^\mu p_1^\nu p_2^\kappa p_0^\lambda M(s, t), \quad (10)$$

involves (as any process which violates natural parity) the totally antisymmetric  $\epsilon$ -tensor and  $M(s, t)$  is a dimensionless invariant function equal to 1 in the soft-pion limit. The prefactor

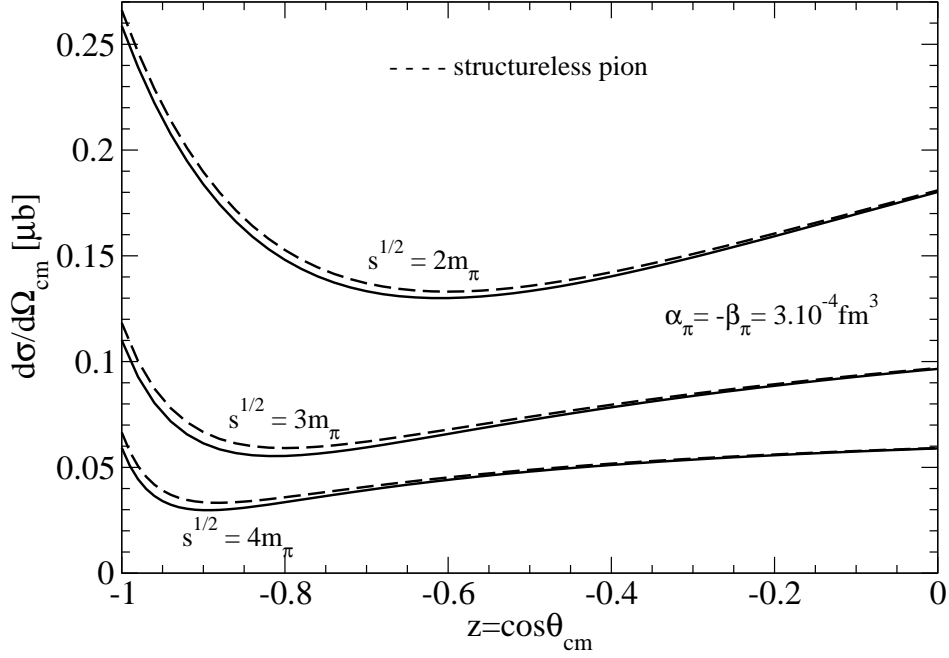


Figure 2: Angular dependence of the differential cross section for charged pion Compton scattering. The full curves are calculated with polarizabilities,  $\alpha_\pi = -\beta_\pi = 3.0 \cdot 10^{-4} \text{ fm}^3$ .

$F_{\gamma 3\pi} = e/(4\pi^2 f_\pi^3) = 9.72 \text{ GeV}^{-3}$  is fixed by the chiral anomaly of QCD (i.e. the anomalous  $VAAA$  rectangle quark diagram). In the effective chiral Lagrangian the  $\gamma 3\pi$ -vertex is provided by the famous Wess-Zumino-Witten term (together with the  $\pi^0 \rightarrow \gamma\gamma$  decay vertex). Neutral pion production in Primakoff reactions serves therefore as test of the QCD chiral anomaly. The low-statistics experiment performed some time ago at Serpukhov has obtained the somewhat high value  $F_{\gamma 3\pi} = (12.9 \pm 1.0) \text{ GeV}^{-3}$  [14]. An improved measurement of  $F_{\gamma 3\pi}$  with much higher statistics has been proposed by the COMPASS collaboration [13] and preliminary data are presently already being analyzed [21].

The total cross section for  $\pi^- \gamma \rightarrow \pi^- \pi^0$  following from the T-matrix in eq.(10) has the form:

$$\sigma_{\text{tot}}(s) = \frac{\alpha(s - m_\pi^2)(s - 4m_\pi^2)^{3/2}}{(4f_\pi)^6 \pi^4 \sqrt{s}} \int_{-1}^1 dz (1 - z^2) |M(s, t)|^2, \quad (11)$$

after substituting  $2t = 3m_\pi^2 - s + z(s - m_\pi^2)\sqrt{1 - 4m_\pi^2/s}$  with  $z$  the cosine of the  $\pi^-$  cms scattering angle. The prefactor  $(s - 4m_\pi^2)^{3/2}$  signals that the final state pions are produced in a relative P-wave. The one-loop corrections for the process  $\pi^- \gamma \rightarrow \pi^- \pi^0$  have been calculated in chiral perturbation theory some time ago in ref.[22]. Together with the tree-level contribution the invariant amplitude  $M(s, t)$  reads:

$$M(s, t)^{(1\text{-loop})} = 1 + \frac{m_\pi^2}{(4\pi f_\pi)^2} \left\{ \frac{4}{3} [J(s) + J(t) + J(u)] - \frac{1}{2} - \ln \frac{m_\pi}{m_\rho} \right\} + \frac{3m_\pi^2}{2m_\rho^2}, \quad (12)$$

where  $s + t + u = 3m_\pi^2$  and we have introduced the loop function:

$$J(4m_\pi^2 x) = \frac{4x}{3} - 1 + (1 - x) \sqrt{1 - \frac{1}{x}} \left\{ \ln |\sqrt{x} + \sqrt{x - 1}| - \frac{i\pi}{2} \theta(x - 1) \right\}. \quad (13)$$

The correction terms to 1 in eq.(12) represent one-loop pion-rescattering in the  $s$ -,  $t$ -, and  $u$ -channel. The last term in eq.(12) corresponds the counterterm contribution estimated via

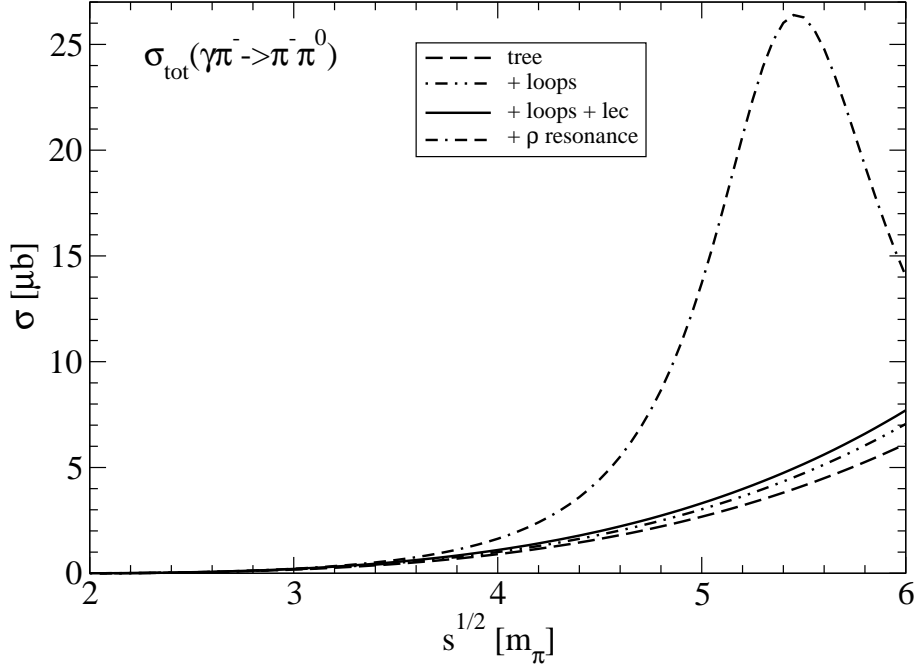


Figure 3: Total cross sections for the reaction  $\pi^- \gamma \rightarrow \pi^- \pi^0$  as a function of the center-of-mass energy  $\sqrt{s}$ .

vector meson exchange and using simplifying symmetry relations for the coupling constants [22].

The three lower curves in Fig. 3 show the total cross section for  $\pi^- \gamma \rightarrow \pi^- \pi^0$  in the region  $2m_\pi < \sqrt{s} < 6m_\pi$ . One sees that the pion-loop and the counterterm corrections each enhance the total cross section by about 10% in comparison to the tree-level approximation. Above center-of-mass energies of  $\sqrt{s} \simeq 4m_\pi$  the effects of the prominent  $\rho(770)$ -resonance can no more be represented by a local counterterm. This is clearly demonstrated by the upper dashed-dotted curve in Fig. 3 which stems from a  $\rho$ -meson exchange model:

$$M(s, t)^{(\rho)} = 1 + \frac{2g_{\rho\pi}G_{\rho\pi\gamma}}{m_\rho^3 F_{\gamma 3\pi}} \left\{ \frac{s}{m_\rho^2 - s - i\sqrt{s}\Gamma_\rho(s)} + \frac{t}{m_\rho^2 - t} + \frac{u}{m_\rho^2 - u} \right\}, \quad (14)$$

including in the  $s$ -channel exchange term an energy-dependent  $\rho$ -meson decay width:

$$\Gamma_\rho(s) = \frac{g_{\rho\pi}^2}{48\pi s} (s - 4m_\pi^2)^{3/2}. \quad (15)$$

Here,  $g_{\rho\pi} = 6.03$  is determined from the empirical decay width  $\Gamma_\rho(m_\rho^2) = 150$  MeV [23] and the coupling constant  $G_{\rho\pi\gamma} \simeq 0.17$  can be inferred from the empirical branching ratio  $\text{Br}(\rho \rightarrow \pi\gamma) = (4.5 \pm 0.5) \cdot 10^{-4}$  [23]. At the  $\rho$ -meson peak the resonant cross section exceeds the one due to chiral low-energy terms by about a factor 5. Potentially, this spectral shape offers a strategy to avoid absolute cross section measurements, namely by covering in the COMPASS experiment the whole region from the  $\rho$ -peak down to threshold. Yet, some model dependence will remain in such a procedure of extracting  $F_{\gamma 3\pi}$ .

## 4 Double pion production

Next, we turn to double neutral pion production  $\pi^- \gamma \rightarrow \pi^- \pi^0 \pi^0$ . This reaction has not been considered so far, mainly because of the lack of any experimental data. With the expected

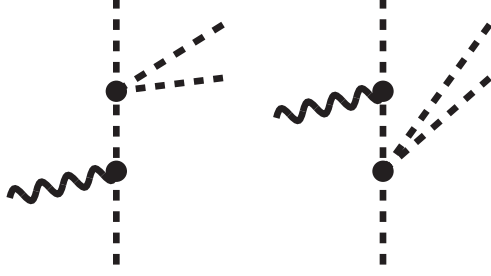


Figure 4: Tree level diagrams for double neutral pion production:  $\pi^- \gamma \rightarrow \pi^- \pi^0 \pi^0$ . In the case of charged pion-pair production,  $\pi^- \gamma \rightarrow \pi^- \pi^+ \pi^-$ , the incoming photon couples also to the other two outgoing pions.

high-statistics of the COMPASS experiment [13] this may change in the near future.

The tree level diagrams for  $\pi^- \gamma \rightarrow \pi^- \pi^0 \pi^0$  are shown in Fig. 4. In the convenient parametrization of the special-unitary matrix field  $U = \sqrt{1 - \vec{\pi}^2/f_\pi^2} + i\vec{\tau} \cdot \vec{\pi}/f_\pi$  a  $\gamma 4\pi$  contact-vertex does not exist. (In other parametrizations its contribution gets canceled by the off-shell part of the  $4\pi$ -vertex.) Moreover, since the left diagram vanishes in Coulomb gauge  $\epsilon \cdot (2p + k) = 0$  we need to evaluate only one single diagram. Performing the polarization sum and three-body phase space integration, we end up with the following expression for total cross section for  $\pi^- \gamma \rightarrow \pi^- \pi^0 \pi^0$ :

$$\begin{aligned} \sigma_{\text{tot}}(s) &= \frac{\alpha}{32\pi^2 f_\pi^4 (s - m_\pi^2)^3} \int_{2m_\pi \sqrt{s}}^{s-3m_\pi^2} dw \sqrt{\frac{s-w-3m_\pi^2}{s-w+m_\pi^2}} (s-w)^2 \\ &\times \left\{ w \ln \frac{w + \sqrt{w^2 - 4m_\pi^2 s}}{2m_\pi \sqrt{s}} - \sqrt{w^2 - 4m_\pi^2 s} \right\}. \end{aligned} \quad (16)$$

Here, the integration variable  $w$  is  $2\sqrt{s}$  times the cms energy of the outgoing  $\pi^-$  and the factor  $(s-w)/f_\pi^2$  originates from the chiral  $\pi^+ \pi^- \rightarrow \pi^0 \pi^0$  interaction.

The lower dashed curve in Fig. 5 shows this total cross section as a function of the center-of-mass energy in the region  $3m_\pi < \sqrt{s} < 7m_\pi$ . Near threshold it grows cubically with the excess energy,  $\sigma_{\text{tot}}(s)_{\text{thr}} = \alpha\sqrt{3}(\sqrt{s} - 3m_\pi)^3/[\pi m_\pi (8f_\pi)^4]$ . With values up to a few microbarn this cross section is still quite sizeable. Note that a resonant  $\rho$ -meson contribution is now not possible, since  $\rho \rightarrow 3\pi$  is forbidden by G-parity.

For the sake of completeness we treat also the charged pion-pair production process  $\pi^- \gamma \rightarrow \pi^- \pi^+ \pi^-$ . Two additional diagrams where the photon couples the other outgoing pions need then to be included. Putting all pieces together, we end up with the following expression for total cross section for  $\pi^- \gamma \rightarrow \pi^- \pi^+ \pi^-$ :

$$\begin{aligned} \sigma_{\text{tot}}(s) &= \frac{\alpha s}{8\pi^3 f_\pi^4 (s - m_\pi^2)^3} \iint_{z^2 < 1} d\omega_1 d\omega_2 \int_{-1}^1 dx \int_0^\pi d\phi \left\{ \frac{q_1^2 (1-x^2)}{(\omega_1 - q_1 x)^2} \right. \\ &\times \left\{ 2[p_0(\sqrt{s} - \omega_2) - \sqrt{s}\omega_1 - k_0 q_2 y]^2 + [k_0 \sqrt{s} - p_0 \omega_1 - k_0 q_1 x]^2 \right\} \\ &+ \frac{2q_1 q_2 (z - xy)}{(\omega_1 - q_1 x)(\omega_2 - q_2 y)} \left\{ [p_0(\sqrt{s} - \omega_2) - \sqrt{s}\omega_1 - k_0 q_2 y] \right. \\ &\times [p_0(\sqrt{s} - \omega_1) - \sqrt{s}\omega_2 - k_0 q_1 x] + 2[k_0 \sqrt{s} - p_0 \omega_2 - k_0 q_2 y] \\ &\left. \left. \times [p_0(\omega_1 + \omega_2) - \sqrt{s}\omega_1 + k_0(q_1 x + q_2 y)] \right\} \right\}, \end{aligned} \quad (17)$$

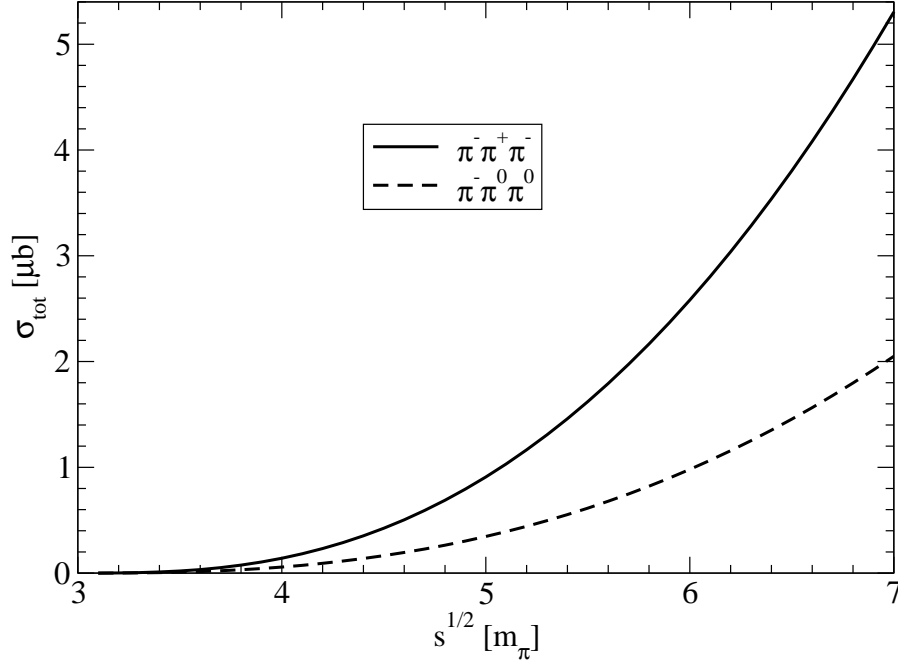


Figure 5: Total cross sections for the double pion production reactions  $\pi^- \gamma \rightarrow \pi^- \pi^0 \pi^0$  and  $\pi^- \pi^+ \pi^-$  as a function of the total center-of-mass energy  $\sqrt{s}$ .

with  $p_0 = (s + m_\pi^2)/(2\sqrt{s})$ ,  $k_0 = (s - m_\pi^2)/(2\sqrt{s})$ ,  $q_{1,2} = \sqrt{\omega_{1,2}^2 - m_\pi^2}$  and

$$q_1 q_2 z = \omega_1 \omega_2 - \sqrt{s}(\omega_1 + \omega_2) + \frac{s + m_\pi^2}{2}, \quad y = xz + \sqrt{(1-x^2)(1-z^2)} \cos \phi. \quad (18)$$

In eq.(17) we have exploited the permutational symmetry of the three-pion phase space in order to reduce the number of independent interference terms in the integrand. This cross section grows in the threshold region also cubically with the excess energy,  $\sigma_{\text{tot}}(s)_{\text{thr}} = \alpha\sqrt{3}(\sqrt{s} - 3m_\pi)^3/[9\pi m_\pi(4f_\pi)^4]$ .

After numerical evaluation of the four-dimensional integral we obtain the total cross sections shown by the upper full curve in Fig. 5. They come out about a factor 2.5 larger than the ones for  $\pi^- \gamma \rightarrow \pi^- \pi^0 \pi^0$ , reaching  $5.3 \mu\text{b}$  at  $\sqrt{s} = 7m_\pi$ . This enhancement can be traced back to the larger number of contributing diagrams.

## 5 Radiative correction: $\pi^- \gamma \rightarrow \pi^- \gamma \gamma$

Finally, we consider the radiative correction process  $\pi^- \gamma \rightarrow \pi^- \gamma \gamma$  to pion Compton scattering. As a smooth background process it interferes also with the neutral pion production  $\pi^- \gamma \rightarrow \pi^- \pi^0$ . Therefore a knowledge of its order of magnitude will be helpful in analyzing the Primakoff data. A representative set of tree diagrams is shown in Fig. 6. These need to be supplemented by diagrams with the two outgoing (right) photons interchanged. We exploit the fact that the coupling of the incoming (left) photon at the bottom of the pion line vanishes in Coulomb gauge and thus are left with 9 non-vanishing diagrams. After performing the triple sums over transversal photon polarizations for the 45 interference terms and applying flux and phase space factors, we end up with a double differential cross section of the form:

$$\frac{d^2\sigma}{d\omega_1 d\omega_2} = \frac{\alpha^3}{8\pi(s - m_\pi^2)} \int_{-1}^1 dx \int_0^\pi d\phi R(\sqrt{s}, m_\pi^2, \omega_1, \omega_2, x, y, z). \quad (19)$$

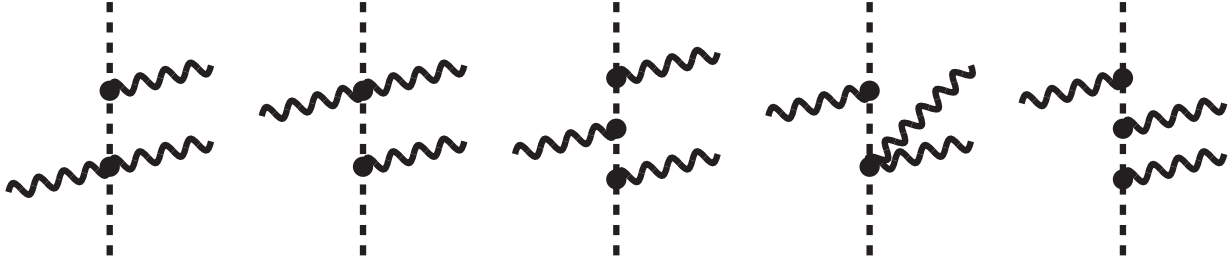


Figure 6: Tree level diagrams for  $\pi^- \gamma \rightarrow \pi^- \gamma \gamma$ . The coupling of the incoming photon at the bottom of the pion line vanishes in Coulomb gauge. Diagrams with the two outgoing photons interchanged are not shown.

Here,  $R(\dots)$  stands for a rational function of its six arguments (which is much too long to be reproduced here).  $\omega_1$  and  $\omega_2$  denote the cms energies of the final state photons and

$$z = 1 - \sqrt{s} \left( \frac{1}{\omega_1} + \frac{1}{\omega_2} \right) + \frac{s - m_\pi^2}{2\omega_1\omega_2}, \quad y = xz + \sqrt{(1-x^2)(1-z^2)} \cos \phi. \quad (20)$$

It is well-known that soft photons with  $\omega_{1,2} \rightarrow 0$  cause a logarithmic infrared divergence of integrated (total) cross section. Therefore, we introduce as a suitable Lorentz-invariant variable the  $\gamma\gamma$  invariant mass squared:

$$m_{\gamma\gamma}^2 = 2\sqrt{s}(\omega_1 + \omega_2) + m_\pi^2 - s = (\sqrt{s} - m_\pi)^2 \cdot \eta^2, \quad (21)$$

related to the sum of the photon energies  $\omega_1 + \omega_2$  and integrate over their half difference  $(\omega_1 - \omega_2)/2$ . For the purpose of a uniform representation we express the two-photon mass spectrum  $d\sigma/d\eta$  in terms of the dimensionless variable  $\eta$  which ranges for all  $\sqrt{s}$  in the unit interval,  $0 \leq \eta \leq 1$ .

Fig. 7 shows the calculated two-photon mass spectrum  $d\sigma/d\eta$  for the process  $\pi^- \gamma \rightarrow \pi^- \gamma \gamma$  at six values of  $\sqrt{s} = (2, 3, 4, 5, 6) m_\pi$ . For  $\eta \rightarrow 0$  the curves diverge as  $d\sigma/d\eta \sim \eta^{-1}$ . It is astonishing that the  $\gamma\gamma$ -spectra possess only a very weak dependence on the total center-of-mass energy  $\sqrt{s}$ . A possible reason herefore could be the similar weak variation of the ratio  $\pi\gamma\gamma$  three-body phase space over flux factor:  $1 + m_\pi^2 s^{-1} - 2m_\pi^2 (s - m_\pi^2)^{-1} \ln(s/m_\pi^2)$ .

We have also considered the interference term of the bremsstrahlung diagrams in Fig. 6 with the  $2\gamma$ -production from  $\pi^0$ -decay. The amplitude for the latter process involves the large scale factor  $2\sqrt{2}\pi f_\pi = 821 \text{ MeV}$  to the fourth power in the denominator. As a consequence of that suppression factor, the integrated interference cross sections (taking e.g.  $0.01 \leq \eta \leq 1$ ) turn out to be extremely small.

Moreover, we show in Fig. 8 (on a logarithmic scale) the total cross sections for the three final states  $\pi^- \gamma$  (full curve),  $\pi^- \pi^0$  (dashed curve), and  $\pi^- \gamma \gamma$  (dashed-dotted curves), altogether. In the latter case these have been obtained (in infrared-regularized form) by integrating the two-photon mass spectrum  $d\sigma/d\eta$  over the interval  $0.01 \leq \eta \leq 1$  and  $0.1 \leq \eta \leq 1$ , respectively. With the exception of the region  $\sqrt{s} < 2.5m_\pi$  very near to the  $\pi^0$ -production threshold, the non-resonant two-photon radiation amounts to at most a few percent correction.

As already mentioned, the two-photon mass spectrum  $d\sigma/d\eta$  of the reaction  $\pi^- \gamma \rightarrow \pi^- \gamma \gamma$  possesses an infrared singularity of the form:

$$\frac{d\sigma}{d\eta} = \frac{\sigma_{\text{ir}}(s)}{\eta} + \mathcal{O}(\eta), \quad (22)$$

in the limit  $m_{\gamma\gamma} \rightarrow 0$ . In practice the leading  $1/\eta$  term provides a good approximation of the two-photon mass spectrum up to  $\eta \simeq 0.25$ . After an elaborate calculation we obtain the

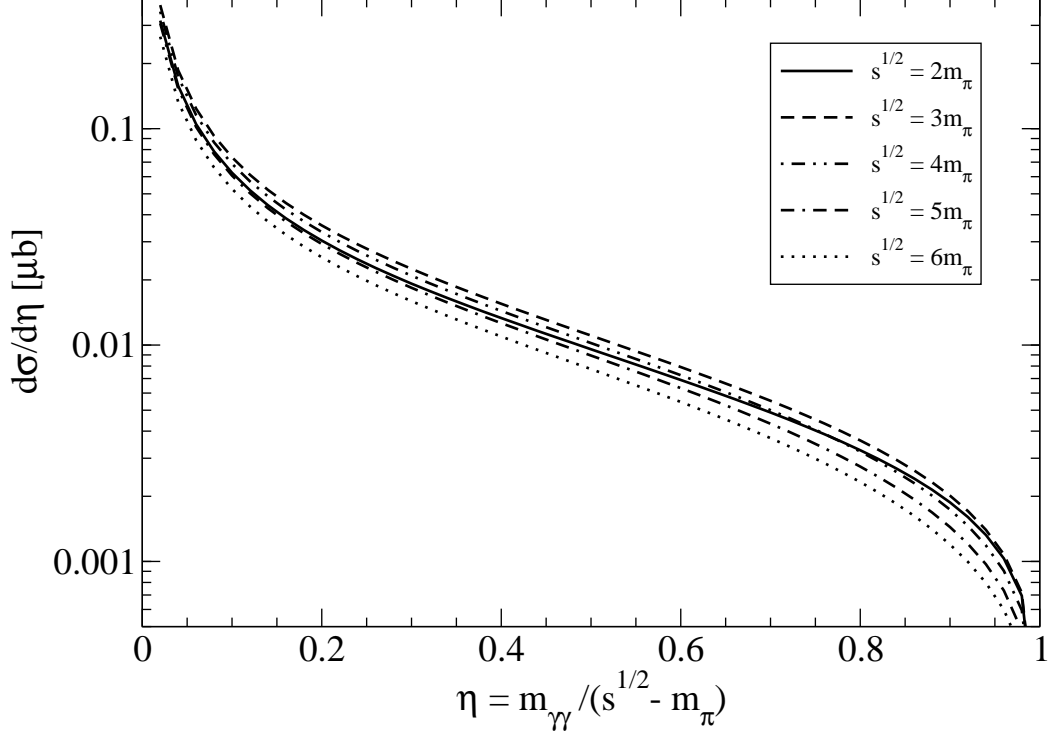


Figure 7: Two-photon mass spectra for the reaction  $\pi^- \gamma \rightarrow \pi^- \gamma \gamma$  as a function of the variable  $\eta = m_{\gamma\gamma}/(\sqrt{s} - m_\pi)$ .

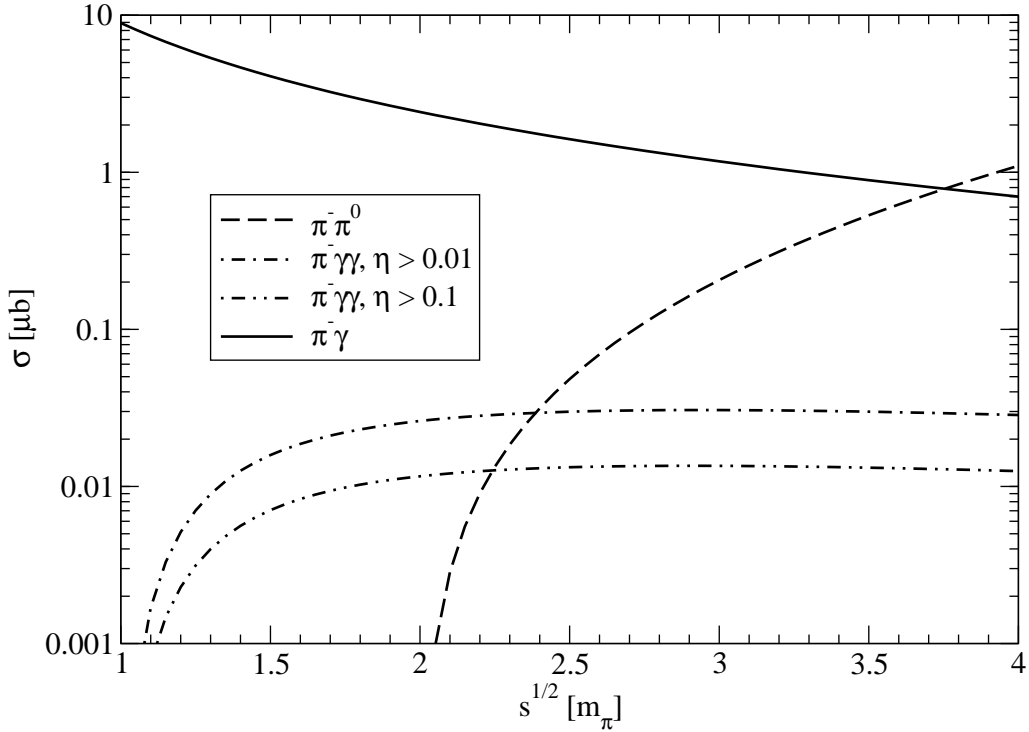


Figure 8: Comparison of total cross sections for the final states  $\pi^- \gamma$ ,  $\pi^- \pi^0$ , and  $\pi^- \gamma \gamma$ . The latter ones have been obtained as infrared-regularized integrals  $\int_{\eta_{\min}}^1 d\eta (d\sigma/d\eta)$  with  $\eta_{\min} = 0.01$  and  $0.1$ .

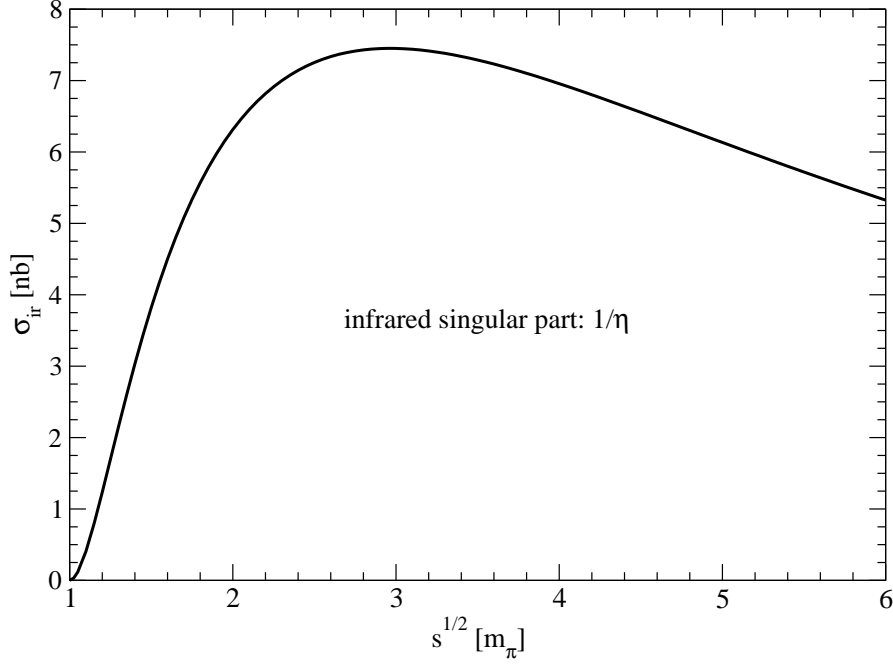


Figure 9: Coefficient  $\sigma_{\text{ir}}(s)$  of the infrared singular part of the two-photon mass spectrum.

following analytical expression for the energy dependent function  $\sigma_{\text{ir}}(s)$  associated with the infrared singular part:

$$\begin{aligned}
\sigma_{\text{ir}}(s) = & \frac{32\alpha^3}{3s} \left\{ -2 + \frac{\hat{s} + 1}{\hat{s} - 1} \ln \hat{s} \right\} \\
& + \frac{16\alpha^3}{3s} \left\{ \frac{\hat{s}^2 + 10\hat{s} + 1}{(\hat{s} - 1)^2} - \frac{6\hat{s}(\hat{s} + 1)}{(\hat{s} - 1)^3} \ln \hat{s} \right\} \left\{ \frac{2\hat{s} - 7\hat{s}^2 - 7}{6(\hat{s} - 1)^2} + \frac{\hat{s}(\hat{s} + 1)}{(\hat{s} - 1)^3} \ln \hat{s} \right\} \\
& + \frac{64\alpha^3}{s} \int_0^1 dx \frac{(1-x)\sqrt{x}[(1-x)^2\hat{s} - x^2][x(\hat{s} - 1)^2 + 2\hat{s}]}{(\hat{s} + x - x\hat{s})^2 \sqrt{x(\hat{s} - 1)^2 + 4\hat{s}}} \\
& \quad \times \ln \frac{\sqrt{x}(\hat{s} - 1) + \sqrt{x(\hat{s} - 1)^2 + 4\hat{s}}}{2\sqrt{\hat{s}}}, \tag{23}
\end{aligned}$$

where  $\hat{s} = s/m_\pi^2$ . The corresponding behavior near threshold is,  $\sigma_{\text{ir}}(s) = 64\alpha^3(\sqrt{s} - m_\pi)^2/(9m_\pi^4)$ , and it comes exclusively from the first term in eq.(23). In order to arrive at this result we have first established in a careful numerical study the 20 non-vanishing contributions to  $\sigma_{\text{ir}}(s)$  from the interference terms of the diagrams in Fig. 6 as well as the identities holding between them. As a result, only six independent interference terms needed to be considered and for these the three-dimensional phase space integral over  $((\omega_1 - \omega_2)/2, x, \phi)$  could then be solved (almost) analytically. In order to bring the integral-term in eq.(23) into its compact form we substituted  $x \rightarrow 1 - 2x$  at the end. Fig. 9 shows the cross section  $\sigma_{\text{ir}}(s)$  as a function of the total center-of-mass energy  $\sqrt{s}$ . Quite interestingly, it reaches a maximum of 7.45 nb at  $\sqrt{s} = 3m_\pi$  and beyond that it decreases slowly as  $s^{-1} \ln(s/m_\pi^2)$ . This behavior is in accordance with the weak  $\sqrt{s}$ -dependence of the two-photon mass spectra  $d\sigma/d\eta$  observed in Fig. 7.

Clearly, in order to establish the complete infrared finiteness of the QED radiative corrections to pion Compton scattering (a la Bloch-Nordsieck), one has to evaluate and include the corresponding one-photon loop diagrams. Work along this line is in progress [24].

# Acknowledgments

We thank S. Paul for triggering this work and for many informative discussions.

# References

- [1] G. Colangelo, J. Gasser, and H. Leutwyler, *Nucl. Phys.* **B603**, 125 (2001); and refs. therein.
- [2] S. Pislak et al., *Phys. Rev.* **D67**, 072004 (2003).
- [3] G. Colangelo, J. Gasser, and H. Leutwyler, *Phys. Rev. Lett.* **86**, 5008 (2001).
- [4] B. Adeva et al., *J. Phys.* **G30**, 1929 (2004).
- [5] J.R. Batley et al., *Phys. Lett.* **B633**, 173 (2006).
- [6] J. Gasser, hep-ph/0710.3048.
- [7] Y.M. Antipov et al., *Phys. Lett.* **B121**, 445 (1983); *Z. Phys.* **C26**, 495 (1985).
- [8] J. Ahrens et al., *Eur. Phys. J.* **A23**, 113 (2005).
- [9] J. Boyer et al., *Phys. Rev.* **D42**, 1350 (1990).
- [10] J. Gasser, M.A. Ivanov, and M.E. Sainio, *Nucl. Phys.* **B745**, 84 (2006); and refs. therein.
- [11] L.V. Filkov and V.L. Kashevarov, hep-ph/0802.0965.
- [12] C.W. Kao, B.E. Norum, and K. Wang, hep-ph/0409081.
- [13] COMPASS Collaboration: P. Abbon et al., hep-ex/0703049.
- [14] Y.M. Antipov et al., *Phys. Rev.* **D36**, 21 (1987).
- [15] G. Fäldt, *Phys. Rev.* **C76**, 014608 (2007).
- [16] G. Fäldt and U. Tengblad, *Phys. Rev.* **C76**, 064607 (2007).
- [17] U. Bürgi, *Nucl. Phys.* **B479**, 392 (1996); and refs. therein.
- [18] J.F. Donoghue and B.R. Holstein, *Phys. Rev.* **D40**, 2378 (1989).
- [19] E. Frlez et al., *Phys. Rev. Lett.* **93**, 181804 (2004).
- [20] C.Q. Geng, I.L. Ho, and T.H. Wu, *Nucl. Phys.* **B684**, 2815 (2004).
- [21] T. Nagel, TU München, E18, private communications.
- [22] J. Bijnens, A. Bramon, and F. Cornet, *Phys. Lett.* **B237**, 488 (1990);  
J. Bijnens, *Int. J. Mod. Phys.* **A8**, 3045 (1993).
- [23] Particle data group: W.M. Yao et al., *J. Phys.* **G 33**, 1 (2006).
- [24] N. Kaiser and J.M. Friedrich, work in progress.